J Braz. Soc. Mech. Sci. Eng. (2017) 39:1735–1744
DOI 10.1007/s40430-016-0644-1

CrossMark

TECHNICAL PAPER

Modeling the coupled effects of surface layer and size effect on the static and dynamic instability of narrow nano-bridge structure

Maryam Keivani[1] · Ali Koochi[2] · Abolfazl Kanani[3] · Hossein M. Navazi[4] · Mohamadreza Abadyan[2]

Received: 9 October 2015 / Accepted: 30 September 2016 / Published online: 13 October 2016

Abstract For modeling the electromechanical behavior of nano-bridge structures with slender narrow-width beam elements, not only the simultaneous effects of surface layer and size dependency should be taken into account but also corrected force models should be considered. In this paper, the instability of a narrow-width nano-bridge is studied based on strain gradient theory and Gurtin–Murdoch surface elasticity. The mid-plane stretching is incorporated in the governing equation as well as corrected force distribution. Using Rayleigh–Ritz method, a parametric analysis is conducted to examine the impacts of surface layer, size dependence, dispersion forces and structural damping on static and dynamic instability voltage of the nano-bridge.

Keywords Nano-bridge · Pull-in instability · Strain gradient theory · Gurtin–Murdoch elasticity · Force correction

Technical Editor: Marcelo A. Savi.

✉ Ali Koochi
A.Koochi@gmail.com

[1] Shahrekord University of Medical Sciences, Shahrekord, Iran

[2] Mechanical Engineering Group, Shahrekord Branch, Islamic Azad University, Shahrekord, Iran

[3] Ionizing and Non-Ionizing Radiation Protection Research Center, Paramedical Sciences School, Shiraz University of Medical Sciences, Shiraz, Iran

[4] Department of Aerospace Engineering, Sharif University of Technology, Tehran, Iran

1 Introduction

With the recent development in the nanotechnology, ultra-small beam-type structures are applied extensively in manufacturing of nano-electromechanical systems (NEMS) such as sensors, probes, actuators, etc. [1–3]. A nano-bridge is one of the essential elements that is highly potential for developing new resonators [4], switches [5], memories [6], and sensors [7]. Figure 1 shows an example of a nano-bridge which comprises a double-clamped flexible electrode over a fixed plate. The length, width and thickness of moveable element are L, b and h, respectively. Applying an electric potential set-up between components causes the movable beam to bend downward to the ground. At a certain voltage, the nano-bridge loses its stability and pulls-in onto the ground electrode. The behavior of nano-structures with wide elements has been examined extensively by previous researches [8–11]. However, few investigators have focused on the instability of narrow-width beam-type systems [12]. For narrow-width nano-bridge, considering suitable force distribution is essential as well as simulating the size dependency and the surface effect.

The nano-scale structural effects, i.e., size dependency should be taken into account in narrow beam-type nano-bridge modeling. A hardening trend is detected in the mechanical behavior of metallic structures when their characteristic dimensions are reduced to sub-micron [13–15]. Also, this trend has been observed in some polymers [16]. The experimental observations report the length scale parameter of Cu-Ag Brass between 0.2 and 20 μm [17]. This parameter is examined to be 4 and 5 μm for copper and nickel, respectively [18]. The abovementioned experiments emphasize that when the characteristic length of the nano-structure is comparable with the internal material length scale, the size dependency is inevitable. The classical

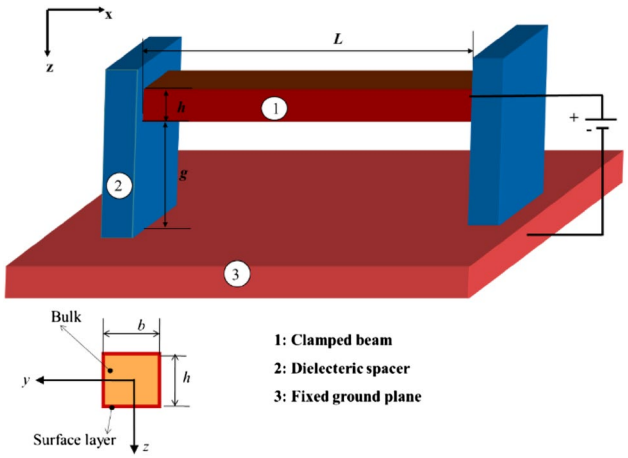

Fig. 1 Schematic view of a nano-bridge

elasticity is not capable for simulating the scale dependency. This phenomenon can be simulated using non-classic theories (e.g., nonlocal elasticity [19], couple stress theory [20], strain gradient theory (SGT) [14], modified couple stress theory (MCST) [21, 22], etc. Previous investigators have examined the mechanical behavior of miniature structures in the context of SGT [23–25]). This theory is more general than the MCST [22] and introduces three material length scale parameters. Indeed, the MCST is a special case of the SGT. In other words, by neglecting the additional higher-order stress components; SGT is degenerated into the MCST. Kong et al. used this size dependent continuum theory to simulate the behavior of an Euler–Bernoulli beam [26]. A new formulation for Timoshenko micro-beams was proposed by Wang et al. [27] based on the SGT.

Besides the scale dependency, the difference between the mechanical performance of surface layer and material might affect the behavior of nano-bridge. Gurtin and Murdoch [28, 29] proposed a continuum theory for incorporating the influence of surface atoms on the mechanical properties of thin solids. The impacts of surface layer on the buckling [30], static bending [31] and oscillation [32] of nano-beams have been examined using Gurtin–Murdoch theory. Liu and Rajapakse have modeled the impacts of surface layer on the mechanical behavior of nano-beams with different cross sections [33]. Recently, Gurtin–Murdoch theory has been engage to estimate the influence of surface energy on the instability parameters of NEMS systems such as nano-bridge [34], cantilever nano-switches [35–37], graphite NEMS [38] and microplates [39].

The aim of the present work is to establish a modified continuum beam model for simulating the pull-in behavior of narrow-width nano-bridge. For the simultaneous effects of surface energy and scale dependency, the SGT is associated with Gurtin–Murdoch elasticity (GME). Moreover, the modified force distribution (i.e., electrical force, Casimir interaction and van der Waals (vdW) force) is used in the simulation. Analytical Rayleigh–Ritz method (RRM) is used to solve the nonlinear constitutive equation.

2 Theory

2.1 Details of SGT

The stored strain energy density in the context of the SGT can be explained as [14]:

$$\bar{U} = \frac{1}{2}\left(\sigma_{ij}\varepsilon_{ij} + p_i\gamma_i + \tau^{(1)}_{ijk}\eta^{(1)}_{ijk} + m^s_{ij}\chi^s_{ij}\right) \tag{1}$$

where ε_{ij}, σ_{ij}, γ_i, ρ_i, $\eta^{(1)}_{ijk}$, $\tau^{(1)}_{ijk}$, χ^S_{ij}, m^S_{ij}, indicate the strain tensor, the classical stress tensor, the dilatation gradient vector, work conjugate to the dilatation gradient vector, the stretch gradient tensor, work conjugate to the stretch gradient tensor, the rotation gradient tensor, work conjugate to the rotation gradient tensor, respectively. These parameters are identified as [14]:

$$\varepsilon_{ij} = \frac{1}{2}\left(u_{i,j} + u_{j,i}\right) \tag{2}$$

$$\gamma_i = \varepsilon_{mm,i} \tag{3}$$

$$\eta^{(1)}_{ijk} = \frac{1}{3}\left(\varepsilon_{jk,i} + \varepsilon_{ki,j} + \varepsilon_{ij,k}\right) - \frac{1}{15}\delta_{ij}\left(\varepsilon_{mm,k} + 2\varepsilon_{mk,m}\right) - \frac{1}{15}\left[\delta_{jk}\left(\varepsilon_{mm,i} + 2\varepsilon_{mi,m}\right) + \delta_{ki}\left(\varepsilon_{mm,j} + 2\varepsilon_{mj,m}\right)\right] \tag{4}$$

$$\chi^s_{ij} = \frac{1}{2}e_{jkl}u_{l,ki} \tag{5}$$

$$\sigma_{ij} = 2\mu\left(\varepsilon_{ij} + \frac{\nu}{1-2\nu}\varepsilon_{mm}\delta_{ij}\right) \tag{6}$$

$$p_i = 2\mu l_0^2\gamma_i \tag{7}$$

$$\tau^{(1)}_{ijk} = 2\mu l_1^2\eta^{(1)}_{ijk} \tag{8}$$

$$m^s_{ij} = 2\mu l_2^2\chi^s_{ij} \tag{9}$$

where ν is Poisson's ratio and μ is shear modulus. Also, l_0, l_1 and l_2 are additional material length scale parameters which appear in the constitutive equations.

2.2 Details of GME

The strain energy in surface layer based on GME (U_S) is written [40]:

$$U_S = \frac{1}{2}\int_0^L \oint_{\partial A} \tau_{ij}\varepsilon_{ij} ds dX \tag{10}$$

The surface constitutive equations are explained as [41]:

$$\begin{aligned} &t_\alpha = \sigma_{\beta\alpha} n_\beta \\ &t_\alpha = -\tau_{\beta\alpha,\beta} \\ &\sigma_{ij} n_i n_j = \tau_{\beta\alpha}\kappa_{\beta\alpha} \end{aligned} \tag{11}$$

where t_α is the traction vector on the surface, $\kappa_{\alpha\beta}$ is the surface curvature tensor, n_i is the outward unit normal to the surface, and $\tau_{\alpha\beta}$ are the in-plane components of the surface stress. The latest is given by:

$$\tau_{\alpha\beta} = \mu_0(u_{\alpha,\beta} + u_{\beta,\alpha}) + (\lambda_0 + \tau_0)u_{p,p}\delta_{\alpha\beta} + \tau_0(\delta_{\alpha\beta} - u_{\beta,\alpha}) \tag{12}$$

where μ_0 and λ_0 are the surface elastic constants, and τ_0 is the residual surface stress. The out-of-plane elements of the surface stress tensor are given by [37].

$$\tau_{n\alpha} = \tau_0(u_{n,\alpha}) \tag{13}$$

2.3 Nonlinear constitutive equation

The displacement field of an Euler–Bernoulli beam is explained as [42]:

$$u_1 = -Z\frac{\partial w(X,t)}{\partial X}, \quad u_2 = 0, \quad u_3 = w(X,t) \tag{14}$$

where w is the centerline deflection of the beam in the Z direction.

2.3.1 Size-dependent strain energy of the bulk

Substituting Eq. (14) in Eqs. (2–9), the nonzero components are determined as:

$$\varepsilon_{11} = -Z\frac{\partial^2 w}{\partial X^2} \tag{15-a}$$

$$\sigma_{11} = -EZ\frac{\partial^2 w}{\partial X^2} \tag{15-b}$$

$$\begin{aligned} &\gamma_1 = -Z\frac{\partial^3 w}{\partial X^3}, \\ &\gamma_3 = -\frac{\partial^2 w}{\partial X^2} \end{aligned} \tag{15-c}$$

$$\begin{aligned} &p_1 = -2\mu l_0^2 Z\frac{\partial^3 w}{\partial X^3}, \\ &p_3 = -2\mu l_0^2\frac{\partial^2 w}{\partial X^2} \end{aligned} \tag{15-d}$$

$$\chi_{12}^s = \chi_{21}^s = -\frac{1}{2}\frac{\partial^2 w}{\partial X^2} \tag{15-e}$$

$$m_{12}^s = m_{21}^s = -\mu l_2^2\frac{\partial^2 w}{\partial X^2} \tag{15-f}$$

$$\begin{aligned} &\eta_{111}^{(1)} = -\frac{2}{5}Z\frac{\partial^3 w}{\partial X^3} \\ &\eta_{113}^{(1)} = \eta_{131}^{(1)} = \eta_{311}^{(1)} = -\frac{4}{15}\frac{\partial^2 w}{\partial X^2} \\ &\eta_{122}^{(1)} = \eta_{212}^{(1)} = \eta_{221}^{(1)} = \eta_{133}^{(1)} = \eta_{313}^{(1)} = \eta_{331}^{(1)} = \frac{1}{5}Z\frac{\partial^3 w}{\partial X^3} \\ &\eta_{223}^{(1)} = \eta_{232}^{(1)} = \eta_{322}^{(1)} = \frac{1}{15}\frac{\partial^2 w}{\partial X^2} \\ &\eta_{333}^{(1)} = \frac{1}{5}\frac{\partial^2 w}{\partial X^2} \end{aligned} \tag{15-g}$$

$$\begin{aligned} &\tau_{111}^{(1)} = -\frac{4}{5}\mu l_1^2 Z\frac{\partial^3 w}{\partial X^3} \\ &\tau_{113}^{(1)} = \tau_{131}^{(1)} = \tau_{311}^{(1)} = -\frac{8}{15}\mu l_1^2\frac{\partial^2 w}{\partial X^2} \\ &\tau_{122}^{(1)} = \tau_{212}^{(1)} = \tau_{221}^{(1)} = \tau_{133}^{(1)} = \tau_{313}^{(1)} = \tau_{331}^{(1)} = \frac{2}{5}\mu l_1^2 Z\frac{\partial^3 w}{\partial X^3} \\ &\tau_{223}^{(1)} = \tau_{232}^{(1)} = \tau_{322}^{(1)} = \frac{2}{15}\mu l_1^2\frac{\partial^2 w}{\partial X^2} \\ &\tau_{333}^{(1)} = \frac{2}{5}\mu l_1^2\frac{\partial^2 w}{\partial X^2} \end{aligned} \tag{15-h}$$

Substituting relations (15) in (1), the strain energy can be defined as:

$$\begin{aligned} U_B = \int_V \bar{U} dV =& \frac{1}{2}\int_0^L \int_A \left\{ EZ^2\left(\frac{\partial^2 w}{\partial X^2}\right)^2 + 2\mu l_0^2 Z^2\left(\frac{\partial^3 w}{\partial X^3}\right)^2 + 2\mu l_0^2 Z^2\left(\frac{\partial^2 w}{\partial X^2}\right)^2 + 2\mu l_2^2 Z^2\left(\frac{\partial^2 w}{\partial X^2}\right)^2 \right. \\ &+ \frac{4}{25}\mu l_1^2 Z^2\left(\frac{\partial^3 w}{\partial X^3}\right)^2 + \frac{48}{225}\mu l_1^2\left(\frac{\partial^2 w}{\partial X^2}\right)^2 + \frac{6}{25}\mu l_1^2 Z^2\left(\frac{\partial^3 w}{\partial X^3}\right)^2 + \frac{1}{75}\mu l_1^2\left(\frac{\partial^2 w}{\partial X^2}\right)^2 + \frac{1}{25}\mu l_1^2\left(\frac{\partial^2 w}{\partial X^2}\right)^2 \left.\right\} dA dX \\ =& \frac{1}{2}\int_0^L \left[\left(EI + 2\mu A l_0^2 + \frac{8}{15}\mu A l_1^2 + \mu A l_2^2\right)\left(\frac{\partial^2 w}{\partial X^2}\right)^2 + A\left(2\mu l_0^2 + \frac{4}{5}\mu l_1^2\right)\left(\frac{\partial^3 w}{\partial X^3}\right)^2 \right] dX \end{aligned} \tag{16}$$

where I is the second moment of area around Y axis and A is the cross-sectional area.

The axial forces results in the stretching energy which is obtained as:

$$U_{ST} = \frac{1}{2}\int_0^L \left(\frac{EA}{2L}\int_0^L \left(\frac{\partial W}{\partial X}\right)^2 dX\right)\left(\frac{\partial W}{\partial X}\right)^2 dX \tag{17}$$

2.3.2 Strain energy in the surface layer

By substituting relation (14) in Eqs. (12, 13), one obtains

$$\begin{aligned}\tau_{XX} &= \tau_0 + E_0\left(-Z\frac{\partial^2 w}{\partial X^2}\right),\\ \tau_{nX} &= \tau_0\frac{\partial u_n}{\partial X}\end{aligned} \tag{18}$$

where $E_0 = \lambda_0 + 2\mu_0$ is the surface elastic modulus. By substituting Eq. (19) in Eq. (10), one obtains the surface energy:

$$U_S = \frac{1}{2}\int_0^L \oint_{\partial A}\left(-\left(\tau_0 + E_0\frac{\partial u_X}{\partial X}\right)Z\frac{\partial^2 w}{\partial X^2} + \tau_0 n_Z^2\left(\frac{\partial w}{\partial X}\right)^2\right)dsdX \tag{19}$$

2.3.3 Work of lateral loads

The work done by lateral loads is gained as:

$$W_{\text{ext}} = \int_0^L \int_0^w F_{\text{ext}}(X,t)dwdX \tag{20}$$

where F_{ext} is the summation of lateral loads, i.e., coulomb and dispersion force.

2.3.4 Kinetic energy and damping loss

The nano-beam is under the influence of a kinetic energy as:

$$T = \frac{1}{2}\int_0^L \int_A \rho\left[\left(\frac{\partial w}{\partial t}\right)^2\right]dAdX \tag{21}$$

In addition, the damping work (W_d) is evinced:

$$_d = \int_0^L c_d w_t w dX \tag{22}$$

where c_d is the damping coefficient.

2.4 External forces

The parallel plates assumption is commonly used to simulate the electrical and dispersion forces. However, in the current study the impacts of finite dimension on the external force distribution are considered. Considering finite dimension correction, the coulomb is acquired as [43]:

$$f_{\text{elec}} = \frac{\varepsilon_0\varepsilon_r}{2}\frac{bV^2}{(g-w)^2}\left[1 + 0.2\left(\frac{g-w}{b}\right)^{0.76} + 0.6\frac{h}{b}\left(\frac{g-w}{h}\right)^{0.76}\right] \tag{23}$$

where $\varepsilon_0 = 8.854 \times 10^{-12}$ c^2 N^{-1} m^{-2} is the vacuum permittivity and ε_r is the relative permittivity of dielectric.

The dispersion forces are classified into the Casimir force for large separation and the *vdW* force for small separation [44–46]. Considering the finite girth the corrected Casimir force is gained as [47]:

$$f_{Cas} = \frac{\pi^2\hbar c b}{240(g-w)^4} + 0.00523\frac{\hbar c}{(g-w)^3} \tag{24}$$

where $\hbar = 1.055 \times 10^{-34} Js$ is the modified Planck's constant and $c = 2.998 \times 10^8$ m/s is the light speed.

The *vdW* force can evaluate by using Lennard-Jones potential [48]. Employing this method the corrected *vdW* force is determined as:

$$f_{vdW} = \frac{\bar{A}b}{6\pi}\left[\frac{1}{(g-w)^3} - \frac{1}{(g+h-w)^3}\right] \tag{25}$$

In the above equation, $\bar{A}$ is the Hamaker constant.

2.5 Dimensionless energy of system

The total energy is defined as:

$$\begin{aligned}\Pi = {} & \frac{1}{2}\int_0^L \int_A \rho\left(\frac{\partial w}{\partial t}\right)^2 dAdX - \int_0^L c_d w_t w dX - \frac{1}{2}\int_0^L \oint_{\partial A}\left(-\left(\tau_0 + E_0 Z\frac{\partial^2 w}{\partial X^2}\right)Z\frac{\partial^2 w}{\partial X^2} + \tau_0 n_Z^2\left(\frac{\partial w}{\partial X}\right)^2\right)dsdX\\ & - \frac{1}{2}\int_0^L \left[\left(EI + 2\mu A l_0^2 + \frac{8}{15}\mu A l_1^2 + \mu A l_2^2\right)\left(\frac{\partial^2 w}{\partial X^2}\right)^2 + I\left(2\mu l_0^2 + \frac{4}{5}\mu l_1^2\right)\left(\frac{\partial^3 w}{\partial X^3}\right)^2\right]dX\\ & - \frac{1}{2}\int_0^L \left(\frac{EA}{2L}\int_0^L \left(\frac{\partial W}{\partial X}\right)^2 dX\right)\left(\frac{\partial W}{\partial X}\right)^2 dX + \int_0^L \int_0^w F_{ext}(X)dwdX\end{aligned} \tag{26}$$

Now, by substituting Eqs. (23–25) in Eq. (26) the non-dimensional total energy is obtained as:

$$\bar{\Pi} = \frac{1}{2}\int_0^1 \rho A\left(\frac{\partial \hat{w}}{\partial \tau}\right)^2 dX - \int_0^1 \int_0^{\hat{w}} \hat{c}\frac{\partial \hat{w}}{\partial \tau} d\hat{w}dx - \frac{1}{2}\int_0^1 t_0\left(\frac{\partial \hat{w}}{\partial x}\right)^2 dx - \frac{1}{2}\int_0^1 \left[6\left(\frac{\gamma}{\eta}\right)^2 \int_0^1 \left(\frac{\partial \hat{w}}{\partial x}\right)^2 dx\right]\left(\frac{\partial \hat{w}}{\partial x}\right)^2 dx$$
$$- \frac{1}{2}\int_0^1 \left[\left(1 + \frac{\mu_s}{15}\left(30\left(\frac{l_0}{l_2}\right)^2 + 8\left(\frac{l_1}{l_2}\right)^2 + 15 + e_0\right)\right)\left(\frac{\partial^2 \hat{w}}{\partial x^2}\right)^2 + \frac{\mu_s}{30(L/h)^2}\left(5\left(\frac{l_0}{l_2}\right)^2 + 2\left(\frac{l_1}{l_2}\right)^2\right)\left(\frac{\partial^3 \hat{w}}{\partial x^3}\right)^2\right]$$
$$+ \int_0^1 \int_0^{\hat{w}} \left(\frac{\alpha^2}{(1-w)^2}\left[1 + (0.2 + 0.6\eta^{0.24})\gamma^{0.76}(1-\hat{w})^{0.76}\right] + \begin{cases} \beta_3\left(\frac{1}{(1-\hat{w})^3} - \frac{1}{\left(1-\hat{w}+\frac{\eta}{\gamma}\right)^3}\right) & vdW \text{ effect} \\ \frac{\beta_4}{(1-\hat{w})^4}(1 + 0.1272\gamma(1-\hat{w})) & \text{Casimir effect} \end{cases} \right) d\hat{w}dx \quad (27)$$

In which the dimensionless parameters are defined as:

$$x = \frac{X}{L} \quad (28\text{-a})$$

$$\hat{w} = \frac{w}{g} \quad (28\text{-b})$$

$$\alpha^2 = \frac{\varepsilon_0 \varepsilon_r b V^2 L^4}{2g^3 EI} \quad (28\text{-c})$$

$$\beta_n = \begin{cases} \frac{\pi C_6 \rho b L^5}{6g^4 EI} & vdW \text{ interaction } (n = 3) \\ \frac{\pi^2 \hbar c b L^4}{240 g^5 EI} & \text{Casimir interaction } (n = 4) \end{cases} \quad (28\text{-d})$$

$$\tau = \sqrt{\frac{EI}{\rho b h L^4}}\, t \quad (28\text{-e})$$

$$e_0 = \frac{E_0 I_0}{EI} \quad (28\text{-f})$$

$$t_0 = \frac{S_0 \tau_0 L^2}{EI} \quad (28\text{-g})$$

$$\mu_s = \frac{12\mu}{E(h/l_2)^2} \quad (28\text{-h})$$

$$\hat{c} = c_d L^2 \sqrt{\frac{1}{\rho b h EI}} \quad (28\text{-i})$$

$$\gamma = \frac{g}{b} \quad (28\text{-j})$$

$$\eta = \frac{h}{b} \quad (28\text{-k})$$

For rectangular section I_0 and S_0 are obtained as:

$$I_0 = \int_S z^2 ds = \frac{1}{2}bh^2 + \frac{1}{6}h^3$$
$$S_0 = \int_S n_z^2 ds = 2b \quad (29)$$

3 Solution method

To study the instability behavior the Rayleigh–Ritz method (RRM) is introduced. In the RRM the beam deflection is assumed as

$$\hat{w}(x) = \sum_{i=1}^{n} q_i(t)\,\phi_i(x) \quad (30)$$

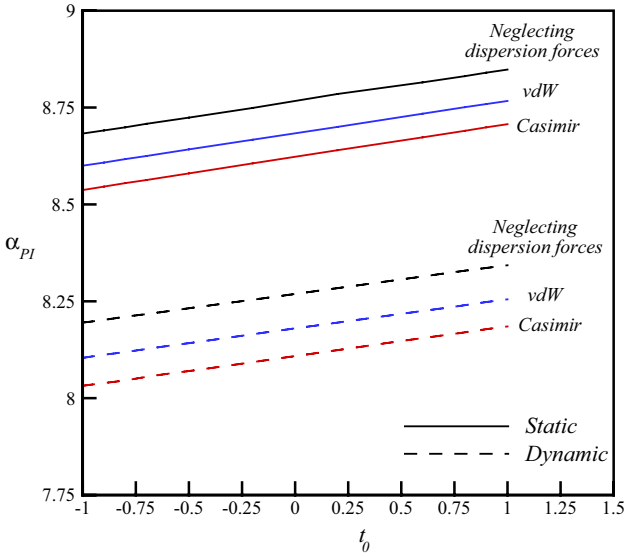

Fig. 2 Impact of surface layer on the pull-in voltage ($\gamma = 0.25$, $\eta = 0.25$, $\beta_n = 1$)

We use the classical mode shapes of the Euler–Bernoulli clamped–clamped beam in the RRM procedure:

$$\phi_i(\xi) = \cosh(\omega_i\xi) - \cos(\omega_i\xi) - \frac{\cosh(\omega_i) - \cos(\omega_i)}{\sinh(\omega_i) - \sin(\omega_i)} (\sinh(\omega_i\xi) - \sin(\omega_i\xi)) \quad (31)$$

where ω_i is the ith root of characteristic equation of the classical clamped beams. For minimize the total energy we must have:

$$\frac{\partial \bar{\Pi}}{\partial q_i} = 0 \quad i = 0, 1, \ldots, N \quad (32)$$

Substituting (27) and (30) into (32), after some mathematical elaborations the following system of ordinary differential equations is achieved:

$$\begin{aligned}
&\ddot{q}_i + \hat{c}\dot{q}_i + \left[1 + \frac{\mu_s}{15}\left(30\left(\frac{l_0}{l_2}\right)^2 + 8\left(\frac{l_1}{l_2}\right)^2 + 15 + e_0\right)\right]\omega_i^4 q_i \\
&- \frac{\mu_s}{30(L/h)^2}\left[5\left(\frac{l_0}{l_2}\right)^2 + 2\left(\frac{l_1}{l_2}\right)^2\right]\int_0^1 \phi_i \frac{\partial^6}{\partial x^6}\left(\sum_{j=1}^{N} q_j\phi_j\right) \\
&- \int_0^1 \phi_i \left\{t_0 + 6\left(\frac{\gamma}{\eta}\right)^2\left[\int_0^1 \left(\sum_{j=1}^{N} q_j \frac{d\phi_j}{dx}\right)^2 dx\right]\sum_{j=1}^{N} q_j \frac{d^2\phi_j}{dx^2}\right\} dx \\
&- \int_0^1 \bar{F}_{ext}\phi_i dx + \frac{\mu_s}{30(L/h)^2}\left(5\left(\frac{l_0}{l_2}\right)^2 + 2\left(\frac{l_1}{l_2}\right)^2\right)\frac{\partial^3}{\partial X^3}\left(\sum_{j=1}^{N} q_j\phi_j\right)\frac{d^2\phi_i}{dX^2}\Bigg|_{x=1} \\
&- \frac{\mu_s}{30(L/h)^2}\left(5\left(\frac{l_0}{l_2}\right)^2 + 2\left(\frac{l_1}{l_2}\right)^2\right)\frac{\partial^3}{\partial X^3}\left(\sum_{j=1}^{N} q_j\phi_j\right)\frac{d^2\phi_i}{dX^2}\Bigg|_{x=0} = 0 \qquad i = 1, 2, .., N
\end{aligned} \quad (33)$$

where

$$\bar{F}_{\text{exr}} = \frac{\alpha^2}{\left(1 - \sum_{j=1}^{N} q_j\phi_j\right)^2}\left[1 + (0.2 + 0.6\eta^{0.24})\gamma^{0.76}\left(1 - \sum_{j=1}^{N} q_j\phi_j\right)^{0.76}\right] + \begin{cases} \beta_3\left(\frac{1}{\left(1 - \sum_{j=1}^{N} q_j\phi_j\right)^3} - \frac{1}{\left(1 - \sum_{j=1}^{N} q_j\phi_j + \frac{\eta}{\gamma}\right)^3}\right) & \text{vdW effect} \\ \frac{\beta_4}{\left(1 - \sum_{j=1}^{N} q_j\phi_j\right)^4}\left(1 + 0.1272\gamma\left(1 - \sum_{j=1}^{N} q_j\phi_j\right)\right) & \text{Casimir effect} \end{cases} \quad (34)$$

where N is the number of assumed terms in the RRM. Finally, the obtained system of differential equation is solved numerically.

4 Results and discussion

In this section the impacts of size dependency, surface layer and dispersion forces on pull-in behavior of nano-bridge are studied. The size parameters are considered as $l_0 = l_1 = l_2$.

Figure (2) illustrates the impacts of surface layer and dispersion forces on the static and dynamic instability voltage of nano-bridge. In this figure the size effect is neglected and $\gamma = \eta = 0.25$. Figure 2 reveals that an augment in the surface residual stress parameter, t_0, results in enhancing the pull-in voltage. Figure 2 also demonstrates that surface stress may cause softening or hardening effect depends on its sign. For materials with negative surface stress this effect induces a softening effect, i.e., detracts the instability voltage. In contrast, for materials with positive surface stress this effect induces a hardening effect,. i.e., increases the instability voltage. In addition, Fig. 2 shows that incorporating the Casimir and *vdW* forces enhances the instability voltage.

The impacts of the scale dependency on the static and dynamic instability voltage of nano-beam are shown in Fig. 3. This figure demonstrates that the scale parameter (l_2/h) results in increasing the pull-in voltage. It is worth to noting that an increase in *l2*/h is responsible for size effect enhancement. This means the scale dependency leads

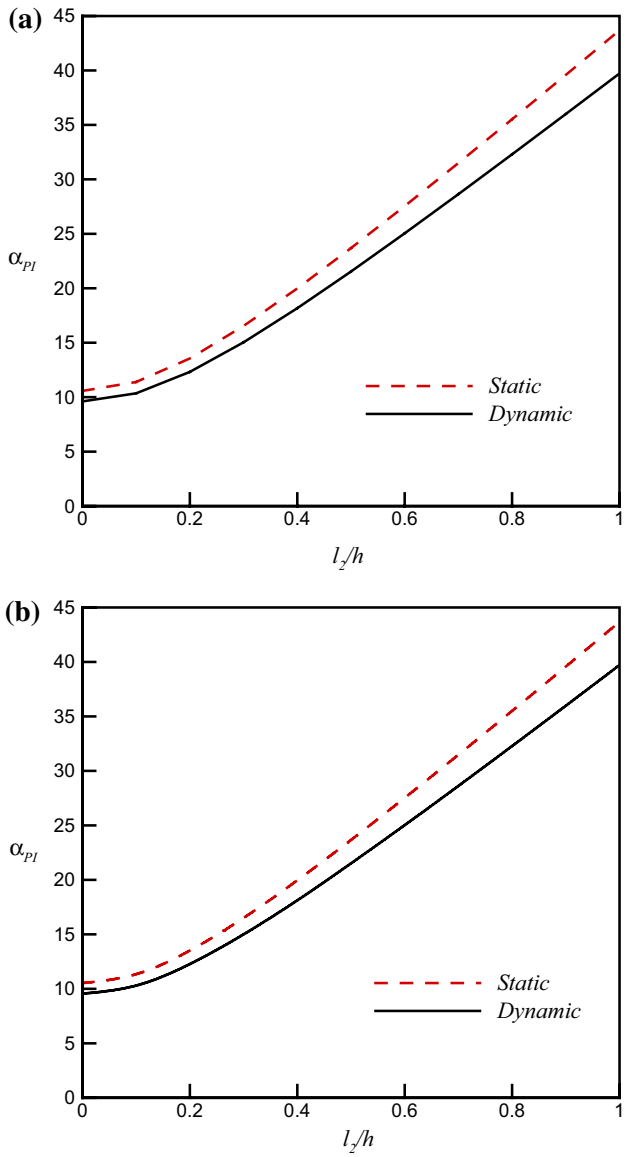

Fig. 3 Impact of size dependency on the static pull-in voltage (neglecting surface effects); **a** *vdW*, **b** Casimir ($\gamma = 0.25$, $\eta = 0.25$, $\beta_n = 1$)

a hardening effect which grows the elastic resistance and consequently enhances the pull-in voltage. Figure 3 reveals that an increase in the beam thickness reduces the size effect.

Figure 4 shows the dynamic response of nano-bridge. In this figure the damping is assumed to be 0.5, i.e., $\hat{c} = 0.5$. This figure demonstrates that the nano-bridge vibrations converge to the focus point by considering the damping. Figure 4 reveals that the second equilibrium point is unstable saddle point. When the applied voltage achieves the pull-in voltage, the trajectories diverge and the nano-bridge becomes unstable.

Wang and Wang [49] studied the influence of surface layer on the behavior of a nano-bridge. Table 1 shows the geometrical parameter and material properties of their case study. In Ref. [49] the linear fringing field for electrical force is assumed and the influence of dispersion forces and size dependency were ignored. Figure 5 shows the variation of mid-point bending of the nano-bridge for various external voltages from zero to pull-in voltage. This figure illustrates that, by ignoring the size effect for both classical theory and surface elasticity the results of the presented model are in very close to the results of Ref. [49]. However, by considering the size effect the beam deflections are decreased and pull-in voltage is increased significantly.

5 Conclusion

In this paper, the electromechanical instability of nano-bridge was simulated based on the SGE and GME. Also, the effect of limited dimension correction on the electrical field, *vdW* attraction and Casimir force was considered. The presented nonlinear model is able to simulate the influences of both surface effect and size dependency on the behavior of nano-bridges. It was found that for positive surface stress, the impact of surface layer enhances the pull-in voltage. However, for materials with negative surface stress, the surface effect reduces the pull-in voltage.

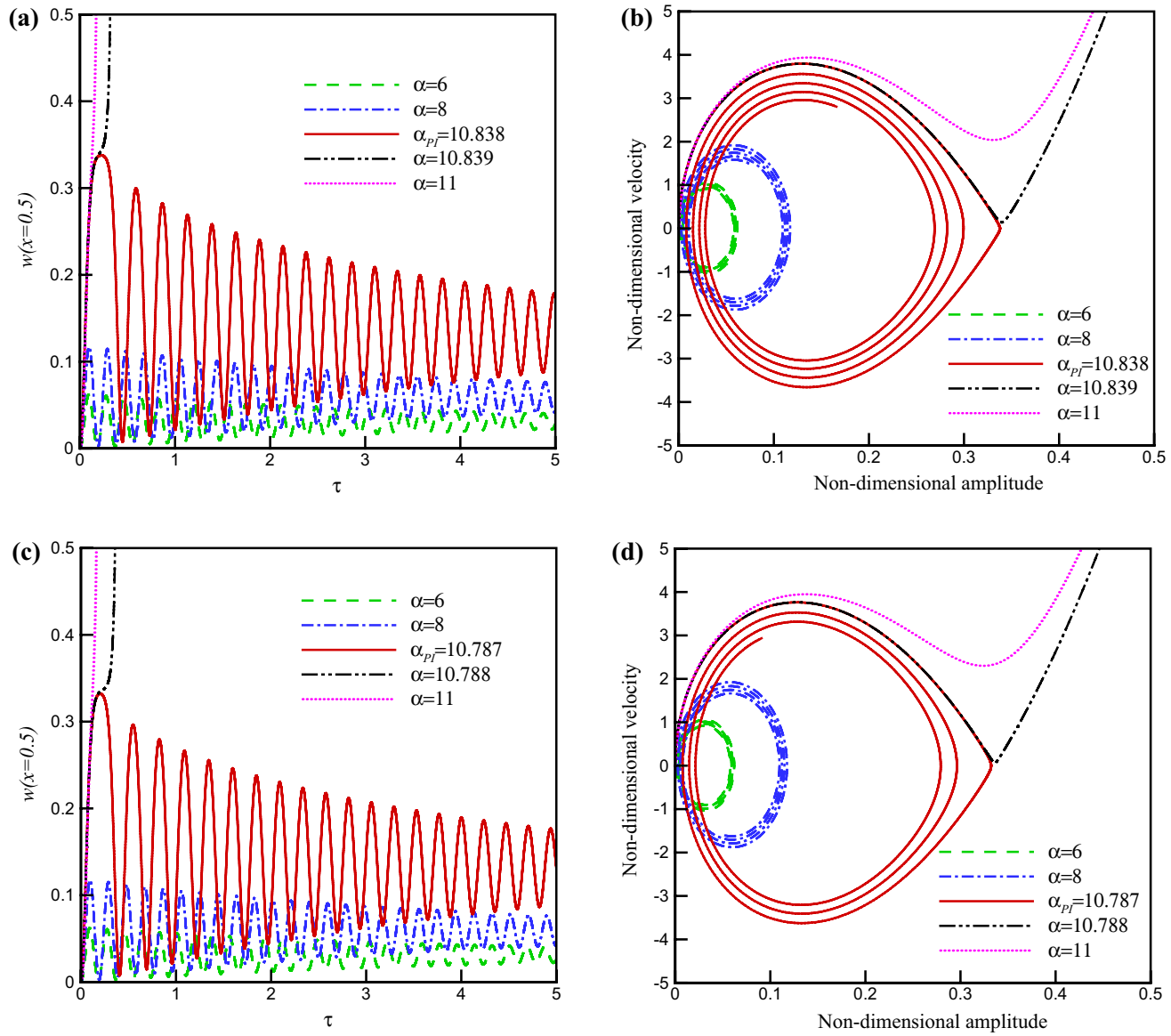

Fig. 4 Impact of damping parameter on the dynamic behavior of nano-bridge (l/h = 0.1; $t_0 = 0.1$, $e_0 = 0.1$, $\beta_n = 1$) **a** time history, *vdW*; **b** phase plane, *vdW*; **c** time history, Casimir; **d** phase plane, Casimir

Table 1 Geometrical parameters and material properties of nano-bridge studied by Wang and Wang [49]

Material properties				Geometrical parameters			
Young's modulus (E)	Poisson's ratio (ν)	Surface elasticity (E_0)	Surface residual stress (τ_0)	Length (L)	Thickness (h)	Width (b)	Initial gap (g)
76 Gpa	0.3	1.22 N/m	0.89 N/m	1 μm	50 nm	5 h	50 nm

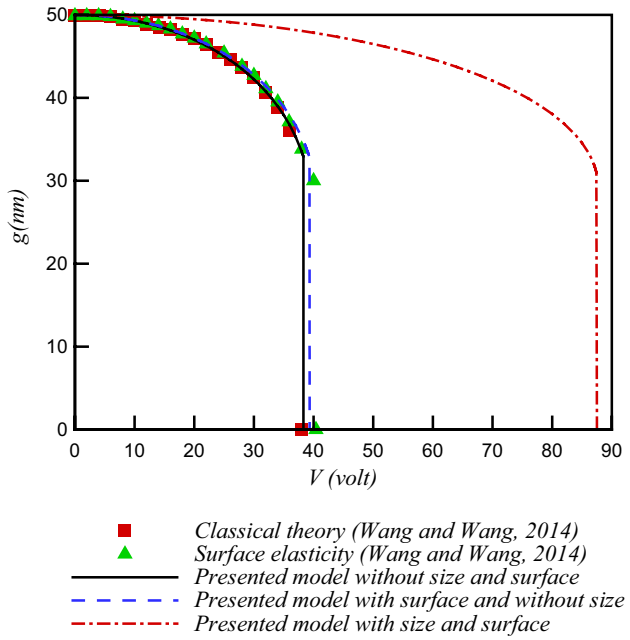

Fig. 5 Mid-plane displacement of nano-bridge as a function of applied voltages

The size effect always increases the instability voltage of nano-bridge while dispersion forces decreases the instability voltage. The dynamic instability voltage of nano-bridge is lower than its static pull-in voltage as the result of inertia forces.

References

1. Rieth M, Schommers W (2006) Handbook of theoretical and computational nanotechnology.American Scientific Publishers, Los Angeles
2. Sedighi HM, Shirazi KH (2013) Vibrations of micro-beams actuated by an electric field via parameter expansion method. Acta Astronaut 85:19–24
3. Duan JS, Rach R (2013) A pull-in parameter analysis for the cantilever NEMS actuator model including surface energy, fringing field and Casimir effects. Int J Solids Struct 50:3511–3518
4. Muñoz-Gamarra JL, Alcaine P, Marigó E, Giner J, Uranga A, Esteve J, Barniol N (2013) Integration of NEMS resonators in a 65 nm CMOS technology. Microelectron Eng 110:246–249
5. Dragoman M, Dragoman D, Coccetti F, Plana R, Muller AA (2009) Microwave switches based on graphene. J Appl Phys 105:054309
6. Uranga A, Verd J, Marigó E, Giner J, Muñóz-Gamarra JL, Barniol N (2013) Exploitation of non-linearities in CMOS-NEMS electrostatic resonators for mechanical memories. Sens Actuators A 197:88–95
7. Hierold C, Jungen A, Stampfer C, Helbling T (2007) Nano electromechanical sensors based on carbon nanotubes. Sens Actuators A 136:51–61
8. Osterberg GPM (2007) Application of the generalized differential quadrature method to the study of pull-in phenomena of MEMS switches. Microelectromechanical Syst J 16:1334–1340
9. Beni YT, Koochi A, Abadyan M (2011) Theoretical study of the effect of Casimir force, elastic boundary conditions and size dependency on the pull-in instability of beam-type NEMS. Physica E 43:979–988
10. Noghrehabadi A, Beni YT, Koochi A, Kazemi AS, Yekrangi A, Abadyan M, Abadi MN (2011) Closed-form approximations of the pull-in parameters and stress field of electrostatic cantilever nano-actuators considering van der Waals attraction. Procedia Eng 10:3750–3756
11. Mobki H, Rezazadeh G, Sadeghi M, Vakili-Tahami F, Seyyed-Fakhrabadi MM (2013) A comprehensive study of stability in an electro-statically actuated micro-beam. Int J Non-Linear Mech 48:78–85
12. Koochi A, Hosseini-Toudeshky H (2015) Coupled effect of surface energy and size effect on the static and dynamic pull-in instability of narrow nano-switches. Int J Appl Mech 7(4):1550064
13. Fleck NA, Muller GM, Ashby MF, Hutchinson JW (1994) Strain gradient plasticity: theory and experiment. Acta Metall Mater 42:475–487
14. Lam DCC, Yang F, Chong ACM, Wang J, Tong P (2003) Experiments and theory in strain gradient elasticity. J Mech Phys Solids 51:1477–1508
15. McFarland AW, Colton JS (2005) Role of material microstructure in plate stiffness with relevance to microcantilever sensors. J Micromech Microeng 15(5):1060–1070
16. Chong ACM, Lam DCC (1999) Strain gradient plasticity effect in indentation hardness of polymers. J Mater Res 14(10):4103–4110
17. Al-Rub RKA, Voyiadjis GZ (2004) Determination of the material intrinsic length scale of gradient plasticity theory. Int J Multiscale Comput Eng 2(3):377–400
18. Wang W, Huang Y, Hsia KJ, Hu KX, Chandra A (2003) A study of microbend test by strain gradient plasticity. Int J Plast 19:365–382
19. Eringen AC, Edelen DGB (1972) On nonlocal elasticity. Int J Eng Sci 10:233–248
20. Ejike UB (1969) The plane circular crack problem in the linearized couple-stress theory. Int J Eng Sci 7:947–961
21. Kong S (2013) Size effect on pull-in behavior of electrostatically actuated microbeams based on a modified couple stress theory. Appl Math Model 37:7481–7488
22. Yang FACM, Chong ACM, Lam DCC, Tong P (2002) Couple stress based strain gradient theory for elasticity. Int J Solids Struct 39:2731–2743
23. Wang B, Zhou S, Zhao J, Chen X (2012) Pull-in instability of circular plate mems: a new model based on strain gradient elasticity theory. Int J Appl Mech 4:1250003
24. Ansari R, Gholami R, Mohammadi V, Shojaei MF (2013) Size-dependent pull-in instability of hydrostatically and electrostatically actuated circular microplates. J Comput Nonlinear Dyn 8:021015
25. Mohammadi V, Ansari R, Shojaei MF, Gholami R, Sahmani S (2013) Size-dependent dynamic pull-in instability of hydrostatically and electrostatically actuated circular microplates. Nonlinear Dyn 73:1515–1526
26. Kong S, Zhou S, Nie Z, Wang K (2009) Static and dynamic analysis of micro beams based on strain gradient elasticity theory. Int J Eng Sci 47:487–498
27. Wang B, Zhao J, Zhou S (2010) A micro scale Timoshenko beam model based on strain gradient elasticity theory. Eur J Mech A/Solids 29:591–599
28. Gurtin ME, Murdoch AI (1975) A continuum theory of elastic material surfaces. Arch Ration Mech Anal 57:291–323
29. Gurtin ME, Murdoch AI (1978) Surface stress in solids. Int J Solids Struct 14:431–440

30. Wang GF, Feng XQ (2009) Surface effects on buckling of nanowires under uniaxial compression. Appl Phys Lett 94:141913
31. He J, Lilley CM (2008) Surface effect on the elastic behavior of static bending nanowires. Nano Lett 8:1798–1802
32. Yan Z, Jiang LY (2011) The vibrational and buckling behaviors of piezoelectric nanobeams with surface effects. Nanotechnology 22:245703
33. Liu C, Rajapakse RKND (2010) Continuum models incorporating surface energy for static and dynamic response of nanoscale beams. IEEE Trans Nanotechnol 9(4):422–431
34. Fu Y, Zhang J (2011) Size-dependent pull-in phenomena in electrically actuated nanobeams incorporating surface energies. Appl Math Model 35:941–951
35. Ma JB, Jiang L, Asokanthan SF (2010) Influence of surface effects on the pull-in instability of NEMS electrostatic switches. Nanotechnology 21:505708
36. Koochi A, Hosseini-Toudeshky H, Ovesy HR, Abadyan M (2013) Modeling the influence of surface effect on instability of nano-cantilever in presence of van der Waals force. Int J Struct Stab Dyn 13:1250072
37. Koochi A, Kazemi A, Khandani F, Abadyan M (2012) Influence of surface effects on size-dependent instability of nano-actuators in the presence of quantum vacuum fluctuations. Phys Scr 85:035804
38. Rokni H, Lu W (2013) A continuum model for the static pull-in behavior of graphene nanoribbon electrostatic actuators with interlayer shear and surface energy effects. J Appl Phys 113:153512
39. Ansari R, Sahmani S (2011) Surface stress effects on the free vibration behavior of nanoplates. Int J Eng Sci 49:1204–1215
40. Gao XL, Mahmoud FF (2014) A new Bernoulli-Euler beam model incorporating microstructure and surface energy effects. Z Angew Math Phys 65:393–404
41. Zhou S, Gao XL (2013) Solutions of half-space and half-plane contact problems based on surface elasticity. Z Angew Math Phys 64:145–166
42. Dym CL, Shames IH (1984) Solid mechanics: a variational approach. Railway Publishing House, Beijing
43. Batra RC, Porfiri M, Spinello D (2006) Electromechanical model of electrically actuated narrow microbeams. Microelectromechanical Systems, Journal of 15:1175–1189
44. Klimchitskaya GL, Mohideen U, Mostepanenko VM (2000) Casimir and van der Waals forces between two plates or a sphere (lens) above a plate made of real metals. Phys Rev A 61:062107
45. Boström M, Sernelius BE (2000) Fractional van der Waals interaction between thin metallic films. Phys Rev B 61:2204
46. Israelachvili JN, Tabor DRFS (1972) The measurement of van der Waals dispersion forces in the range 1.5 to 130 nm. In: Proceedings of the Royal Society of London A: Mathematical, Physical and Engineering Sciences, Vol. 331, No. 1584, p 19–38
47. Gies H, Klingmüller K (2006) Casimir edge effects. Phys Rev Lett 97:220405
48. Lennard-Jones JE (1930) Perturbation problems in quantum mechanics. In: Proceedings of the Royal Society of London. Series A, Containing Papers of a Mathematical and Physical Character 598-615
49. Wang KF, Wang BL (2014) Influence of surface energy on the non-linear pull-in instability of nano-switches. Int J Non-Linear Mech 59:69–75